Plasmonics (2007) 2:55–64
DOI 10.1007/s11468-007-9027-x

Application of Surface-Enhanced Raman Spectroscopy for Detection of Beta Amyloid Using Nanoshells

Hope T. Beier · Christopher B. Cowan · I-Hsien Chou · James Pallikal · James E. Henry · Melodie E. Benford · Joseph B. Jackson · Theresa A. Good · Gerard L. Coté

Received: 20 February 2007 / Accepted: 27 April 2007 / Published online: 6 June 2007

Abstract Currently, no methods exist for the definitive diagnosis of AD premortem. β-amyloid, the primary component of the senile plaques found in patients with this disease, is believed to play a role in its neurotoxicity. We are developing a nanoshell substrate, functionalized with sialic acid residues to mimic neuron cell surfaces, for the surface-enhanced Raman detection of β-amyloid. It is our hope that this sensing mechanism will be able to detect the toxic form of β-amyloid, with structural and concentration information, to aid in the diagnosis of AD and provide insight into the relationship between β-amyloid and disease progression. We have been successfully able to functionalize the nanoshells with the sialic acid residues to allow for the specific binding of β-amyloid to the substrate. We have also shown that a surface-enhanced Raman spectroscopy response using nanoshells is stable and concentration-dependent with detection into the picomolar range.

H. T. Beier (✉) · I.-H. Chou · M. E. Benford · G. L. Coté
Department of Biomedical Engineering, Texas A&M University,
337 Zachry Engineering Center, 3120 TAMU,
College Station, TX 77843-3120, USA
e-mail: hopebeier@neo.tamu.edu

C. B. Cowan · J. Pallikal · J. E. Henry · T. A. Good
Department of Chemical & Biochemical Engineering,
University of Maryland Baltimore County,
Baltimore, MD, USA

J. B. Jackson
Nanospectra Biosciences, Inc.,
Houston, TX, USA

Present address:
J. E. Henry
Department of Chemical Engineering, Louisiana State University,
Baton Rouge, LA, USA

Keywords Surface-enhanced Raman spectroscopy · SERS · Raman spectroscopy · Nanoshells · β-amyloid · Alzheimer's disease · Congo red · Self-assembled monolayer

Introduction

Since Alois Alzheimer first discovered the pathology of the disease bearing his appellation in 1906, the number of people diagnosed with Alzheimer's disease (AD) has been on the rise [1]. Alzheimer's disease, a neurodegenerative disease and the most common cause of dementia, affects 4.5 million people according to the 2000 US census [2]. Due to various factors, such as longer life expectancy, the aging of the Baby boomers, and the subsequent increase of the number of people in the oldest age group (>65), the incidence of AD is expected to triple to 13.2 million by the year 2050 [2–5]. The economic impact of AD is staggering. With an annual cost of over $100 billion per year, AD is the third most costly disease in the USA after heart disease and cancer [6]. In recent years, there has been great interest and progress made in the development of molecular level strategies to target steps in the pathogenesis of AD [7–18], with the expectation that even a modest delay of onset of AD of as little as 5 years would result in a 50% reduction in the number of AD patients [19]. However, if these new molecular therapeutics are to be successfully applied, a definitive premortem diagnosis of AD is necessary.

Premortem diagnosis of AD is only probable and is based on in vivo imaging of the brain with magnetic resonance imaging or functional positron emission tomography, along with tests of cognitive and psychological function [20–22]. Alzheimer's disease can only be diagnosed definitively by identifying extracellular amyloid plaques composed of amyloid-β (Aβ) and neurofibrillary tangles, which consist

of tau proteins, in postmortem central nervous system tissue [5, 23–30]. The main constituent of the neuritic plaques is the 39–43 amino acid peptide, β-amyloid (Aβ). The presence of neurofibrillary tangles in the absence of neuritic plaques indicates the pathogenesis of other, less common neurodegenerative diseases. On the same note, neuritic plaques, in the absence of neurofibrillary tangles, can be found in brains with no detectable neuritic dystrophy; these are known as diffuse, or preamyloid, plaques. These diffuse plaques can develop 20 years before the person shows symptoms of dystrophic neurons [3, 5, 24, 27]. For many patients, it is difficult to determine cognitively whether the patient has AD or only mild cognitive impairment, a disease which may progress to AD or remain as a benign form of normal aging [23, 26, 30].

With the goal of developing a means of diagnosing AD premortem, many groups are looking into the detection of the two proteins, tau and Aβ, that are associated with the disease postmortem. While it is not certain that levels of these proteins will correlate with AD, it is speculated that a means of detecting structure-specific forms of Aβ in cerebral spinal fluid (CSF) may be used as a biomarker for AD. Soluble oligomers of Aβ act as ligands on the cell membrane, consequently earning the name Aβ-derived diffusible ligand (ADDL), triggering a cascade of events that many hypothesize brings about neuritic dystrophy and neuronal death. ADDLs specifically have high-affinity binding with gangliosides containing multiple sialic acid residues. Studies show that intermediate oligomer forms of the Aβ protein such as ADDLs, rather than monomeric or fibril forms, disrupt learning and behavior and are more likely to be the cause of the disease toxicity [5, 7, 24, 27–29, 31–36]. Some research groups are looking into the detection of ADDLs through the use of antibodies specific to this protein. Haes et al. have instituted the use of localized surface plasmon resonance nanosensors to detect anti-ADDL antibodies and ADDLs [37, 38]. This approach was able to determine the concentration of ADDLs in the diseased brain to be around 1 pM, with a larger concentration of ADDLs in the CSF of AD patients as compared to non-AD patients. Georganopoulou et al. used bio-barcode technology for the specific detection of ADDLs in CSF [39]. This approach was able to detect ADDLs into the femtomolar range and was important in demonstrating the correlation of elevated ADDL levels with AD. However, these two approaches were specific only to ADDLs, one form of the many oligomeric forms of Aβ that could be indicative of AD. Development of a sensor platform that enables the rapid and selective detection of ADDLs along with other Aβ oligomers and fibril species that may contribute to AD pathology would be a valuable tool in the study of AD and the development of premortem diagnostics for this disease.

The Raman spectrum is considered a useful tool for detection of bioanalytes because it provides an optical fingerprint of the molecules in question. Traditional Raman spectroscopy, however, is an ineffective tool for bioanalyte detection, especially at trace concentrations, because a relatively low number of photons are Raman, or inelastically, scattered as compared to the number of photons that are Rayleigh, or elastically, scattered. To overcome this problem, the use of surface-enhanced Raman spectroscopy (SERS) has been instituted. SERS provides significant enhancement of the Raman intensity, on the order of 10^6 to 10^{14} times, through electromagnetic field enhancement and chemical enhancement that increases the Raman cross section of the individual molecule when the molecule of interest is close to a roughened metal [40–46]. These enhancement factors are considered to represent the SERS signal at a Raman-scattered frequency υ_S in Eq. 1 [45, 46].

$$P^{\mathrm{SERS}}(\upsilon_S) = N'\sigma^{\mathrm{R}}_{\mathrm{ads}} I(\upsilon_L)|A(\upsilon_L)|^2|A(\upsilon_S)|^2 \tag{1}$$

In this equation, N' is the number of molecules involved in the SERS process, $\sigma^{\mathrm{R}}_{\mathrm{ads}}$ represents the increased Raman cross section of the adsorbed Raman-active molecules, and $I(\upsilon_L)$ is the intensity of the excitation source. $|A(\upsilon_L)|^2$ and $|A(\upsilon_S)|^2$ are the electromagnetic enhancement factors at the excitation and Raman-scattered frequencies, respectively. Using the approximation of a small sphere of radius r with a complex dielectric constant $\varepsilon(\nu)$ in a surrounding medium with a dielectric constant of ε_0, the enhancement can be estimated as shown in Eq. 2 to produce the total electromagnetic enhancement given in Eq. 3.

$$|A(\upsilon)| \approx \frac{\varepsilon(\upsilon)-\varepsilon_0}{\varepsilon(\upsilon)+2\varepsilon_0}\left(\frac{r}{r+d}\right)^3 \tag{2}$$

$$|A(\upsilon_L)|^2|A(\upsilon_S)|^2 \approx \left|\frac{\varepsilon(\upsilon_L)-\varepsilon_0}{\varepsilon(\upsilon_L)+2\varepsilon_0}\right|^2\left|\frac{\varepsilon(\upsilon_S)-\varepsilon_0}{\varepsilon(\upsilon_S)+2\varepsilon_0}\right|^2\left(\frac{r}{r+d}\right)^{12} \tag{3}$$

In these equations, d is the distance of the analyte molecule from the metal sphere, indicating the very strong spatial dependence of the SERS signal. The enhancement is strongest when the surface plasmons are in resonance with both the excitation and Raman-scattered fields, and this enhancement is dependent, to the fourth power, on the local nanostructure field of the metal. These strong spatial and local nanostructure field dependencies may be producing the small, localized "hot spots" of extremely strong enhancement known to occur with SERS, which give the potential for trace analyte detection but also make the production of reproducible SERS surfaces difficult [45, 46].

Nanoshells are spherical nanoparticles with a dielectric core surrounded by a metal shell with plasmon resonances that can be adjusted by altering the ratio of the core diameter to the shell diameter [47]. Nanoshells have been previously shown to provide significant SERS enhancements of 10^6–10^{10} in the near IR by tuning the plasmon resonance to the excitation laser wavelength [48–50]. Additionally, by controlling the geometry of the nanoshells, the SERS enhancement for a layer of nonresonant molecules bound to the surface of the nanoshells can be controlled with quantitative agreement between theoretical and experimental results [48]. Solutions of nanoshells are limited by significant reabsorption of the backscattered SERS signal by other nanoshells, which limits the observed SERS enhancement [49]. Thus, it is desired that the nanoshells be deposited onto a substrate to allow for larger SERS enhancements due to the simplified collection geometry. The intensity of the Raman signal from these nanoshell substrates has been shown to have a linear dependence on the density of nanoshells, indicating that the observed SERS signal is dependent on the resonance of single nanoshells with little contribution from aggregates. It is theorized that the interparticle forces between the nanoshells are very strong, resulting in the nanoparticles being either more than a particle radius apart or in direct contact. This direct contact between the nanoshells likely does not allow for the deposition of the adsorbate molecules between the nanoshells. This response is in opposition to the response from solid nanoparticles where the observed SERS signal was minimal until the nanoparticles began to form aggregates on the film [51]. Thus, unlike aggregates of solid nanoparticles where the enhancement is derived from uncontrolled aggregates of particles that produce "hot spots" for SERS enhancement [52], the SERS enhancement from the nanoshells is not dependent on these "hot spots." This feature allows for a uniform substrate where the SERS enhancement can be determined to be a function of the number of the molecules bound to the substrate, not as a function of the degree of enhancement in that one location.

The use of a gold nanoshell film is also advantageous because the surface of gold can be easily modified with the direct linkage of a thiol functional group. To create a surface selective for Aβ, we have instituted the use of a self-assembled monolayer (SAM) of cysteamine bound to sialic acid on the gold nanoshells (Fig. 1). Sialic acid is one of many sugars that make up the glycolipids and glycoproteins on a cell surface. Aβ has been shown to have a high affinity for sialic acid containing gangliosides [7, 29, 53–58] and multivalent sialic acid polymers [18]. Thus, by functionalizing the nanoshell film with sialic acid, we are attempting to mimic the cell surface to create a platform to induce specific binding of Aβ. With Aβ bound specifically to the nanoshell substrates, other confounders found in biological media can be removed, and Congo red can then be bound to the Aβ. Congo red is frequently used to stain amyloid fibrils in tissue and has been shown to bind to the toxic formations of Aβ [59–61]. Congo red also produces more distinct Raman peaks than Aβ; this advantage can be used to more easily determine Aβ concentration and conformation. In this paper, we explore the feasibility of using functionalized nanoshells as a platform for the SERS detection of Aβ to aid in the understanding of AD, with the ultimate goal of creating a sensor for use in a clinical setting for the premortem diagnosis of AD.

Experimental

Materials

Aβ(1–40), with the sequence DAEFRHDSGYEVHHQ KLVFFADVGSNKGAIIGLMVGGVV, was synthesized and purified by BioSource International (Camarillo, CA, USA). Purity as confirmed by mass spectrometry and HPLC was >95%. *N*-hydroxysulfosuccinimide (sulfo-NHS) and 1-ethyl-3-[3-dimethylaminopropyl]carbodiimide hydrochloride (EDC), Iodo-Beads, G-5 desalting columns, and Bolton–Hunter reagent (sulfo-SHPP) were purchased from Pierce Biotechnology (Rockford, IL, USA). ^{125}I was purchased from Amersham Biosciences (Piscataway, NJ, USA). 2-(*N*-morpholino)ethanesulfonic acid (MES) was purchased from Fisher Biotech (Fair Lawn, NJ, USA). All other chemicals were purchased from Sigma-Aldrich (St. Louis, MO, USA).

Substrate preparation

Glass slides were cleaned with potassium hydroxide before being coated with an even layer of poly(vinyl pyridine) (PVP). The nanoshell solution was deposited onto the PVP-

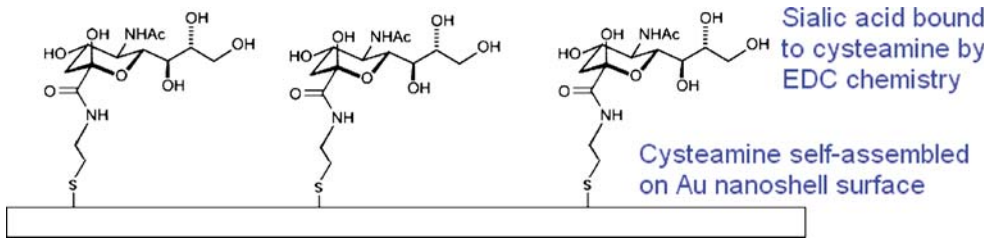

Fig. 1 Scheme showing the self-assembled monolayer bound to the nanoshells. By functionalizing the nanoshells with sialic acid, we create a platform for the specific binding of Aβ, with limited binding of other nonspecific proteins

modified slides and allowed to bind for 3 h. The nanoshells were engineered to maximize the Raman response for a 785-nm laser excitation in an air environment. The nanoshells have a core radius of ~94 nm, with ~18-nm-thick gold shells. These dimensions were determined by comparing the measured absorbance to Mie scattering calculations, and verified by dynamic light scattering. To increase the reflectance of the slides to increase the grazing angle Fourier transform infrared (FTIR) and SERS signals, vapor deposition was used to coat the glass slides with a thin layer of gold prior to PVP deposition.

Nanoshell slides were then prepared for modification by cleaning the slides in a hydrogen peroxide solution for 1.5 h before drying under a gentle N_2 stream. A solution of 1 mM sialic acid, 1 mM cysteamine, 10 mM sulfo-NHS, and 4 mM EDC was prepared in a 0.1-M MES buffer. The pH was adjusted to 5.0 and the solution was allowed to react for 6 h, while being mixed, to ensure proper attachment of the sialic acid to the amine terminal of the cysteamine. Then, 500 μL of the reacted solution was pipetted over the gold nanoshell surface. The thiol functional groups of the cysteamine bound spontaneously to the gold surface of the nanoshells to create a uniform, self-assembled monolayer (Fig. 1).

Determination of binding affinity ($K_{A\beta}$) and surface saturation (N_{sat})

Binding affinity of Aβ to the surfaces was estimated from equilibrium binding isotherms performed using radioiodinated Aβ [18]. Aβ(1–40) was radioiodinated via a modified Bolton Hunter method to preferentially label at the N terminus of the peptide. One hundred nanomoles of sulfo-SHPP was iodinated with 200 μCi of ^{125}I using the IodoBead catalyst for 15 min at pH 8.0 borate buffer in a volume of 140 μL. After removal of the catalyst, 2 nmol (100 μL) of freshly prepared Aβ(1–40) (in water) was added and allowed to react to the iodinated sulfo-SHPP for 3 h at 4°C. The resulting condensation product was separated from free ^{125}I using a G-5 desalting column, employing phosphate buffer as the eluent. The trichloroacetic acid precipitatable activity was determined to be >90%. No attempt was made to remove unlabeled peptide from labeled peptide.

Aprotinin and lysozyme were iodinated directly without using sulfo-SHPP. Two Iodobeads were added to 100 μL PBS, to which 100 μCi ^{125}I (10 μL) was added. Three hundred ninety microliters of either 1 mg/mL of lysozyme or 0.5 mg/mL of aprotinin was incubated in the presence of ^{125}I and Iodobeads for 10 min. Iodinated protein was separated from free ^{125}I using G-5 desalting columns.

Binding assays were carried out by incubating ^{125}I-labeled protein of different concentrations directly with sialic acid-modified surfaces at room temperature for 2 h. Tween-20 was also added at a final concentration of 0.1% to block nonspecific binding. Thereafter, free protein was removed from that bound to the surface by directly pipetting the solution from the surface. Bound protein was recovered from the surface by gently rubbing a 1-cm^2 area of the surface with a cotton swab. Activities of the free protein and bound protein (now attached to the cotton swab) were measured using a Wallac MicroBeta TriLux microplate liquid scintillation counter (Perkin Elmer, Wellesley, MA, USA). Binding constants were determined from these resultant equilibrium binding isotherms by fitting a Langmuir isotherm (Eq. 4) to the data using a nonlinear least squares regression algorithm (KaleidaGraph 3.6, Synergy Software, Reading, PA, USA).

$$N_{\text{bound}} = \frac{[A\beta]_{\text{free}} N_{\text{sat}}}{K_{A\beta} + [A\beta]_{\text{free}}} \tag{4}$$

where N_{bound} is the picomoles of Aβ bound to the surface; $K_{A\beta}$ is the equilibrium dissociation coefficient of Aβ with the surface; $[A\beta]_{\text{free}}$ is the concentration of Aβ in solution at equilibrium; and N_{sat} is the picomoles of Aβ on surface at saturation conditions. The amount of Aβ bound to the surface was normalized by the amount of surface area to which the Aβ bound. Surface area was estimated as the area covered by nanoshells but did not include an estimate of any additional surface area from the nanoshell surfaces.

SERS experiments

Aβ was dissolved in DMSO to a concentration of 10 mg/mL, aliquoted into microcentrifuge tubes containing 5 μL of solution and stored in a −80°C freezer until use. Ninety five microliters of 0.1 M PBS (pH 7.4) was added to the Aβ to create a 0.5-mg/mL (115 μM) solution. The Aβ was then stirred on a rotary stirrer for 24 h at room temperature to form a mixture of oligomers and fibrils before being stepwise diluted to the concentrations of interest. Thirty microliters of Aβ was added to nanoshell surfaces and given 30–45 min to bind before being rinsed 3× with PBS and 1× with deionized water. The slides were then dried with a gentle stream of N_2. Congo red at a concentration of 120 μM in PBS was added to the slides and allowed to bind for 20 min before the slides were rinsed and dried as before.

The SERS analysis was performed on a Renishaw System 1000 Raman Spectrometer (Wotton-under-Edge, UK) coupled to a Leica DMLM microscope (Wetzlar, Germany). A 785-nm GaAlAs diode laser (SDL model XC30) was used as the excitation laser. A 10× objective lens was used to deliver 14.5 mW to the sample with an approximate 10-μm spot size. A 20× objective lens was also used, which delivered 6.22 mW to the sample with an

approximate 5-μm spot size. Raman scans were taken at random locations on the modified nanoshells surfaces and were integrated for 15 or 30 s over the range of 1,623–1,110 cm^{-1}.

Results and discussion

FTIR characterization—cysteamine and EDC chemistry

To confirm that the nanoshells films were functionalized with the specific binding chemistry as intended, FTIR spectra were taken throughout the reaction steps of the sialic acid surface modification. These spectra are shown in Fig. 2. The gold baseline spectrum is representative of the grazing angle spectra taken of only the gold surface before any modification takes place. As we would expect, there is no signal. A spectrum of free sialic, not bound to the surface, is included to illustrate the IR signature associated with the sugar. The gold + linker is representative of the grazing angle spectra taken of the gold surface modified with cysteamine. Chemical signatures can be seen at ~3,000 and 2,800 cm^{-1}, as well as at 3,650 and 1,400 cm^{-1}, which indicates that carbon chain and amine functional groups are present, thus showing that cysteamine attached properly. The gold + linker + EDC/SA is representative of the grazing angle spectra taken of the gold surface that was reacted with cysteamine, which was then reacted with sialic acid through EDC chemistry. Chemical signatures can be seen at ~1,300 and 1,200 cm^{-1} that are indicative of the EDC reaction while preserving the amine and carbon structure associated with the cysteamine attachment. These results indicate that we have functionalized the nanoshells substrates with sialic acid so that they may be used for the specific binding of Aβ to the surfaces. The spectra were taken from slides prepared when we performed the chemistry steps associated with attachment of sialic acid to the surface sequentially; however, similar final spectra were obtained whether attachment was done sequentially or if the cysteamine was reacted with the sialic acid in solution prior to attachment to the surface. For most measurements, we actually prepared surfaces by reacting the cysteamine

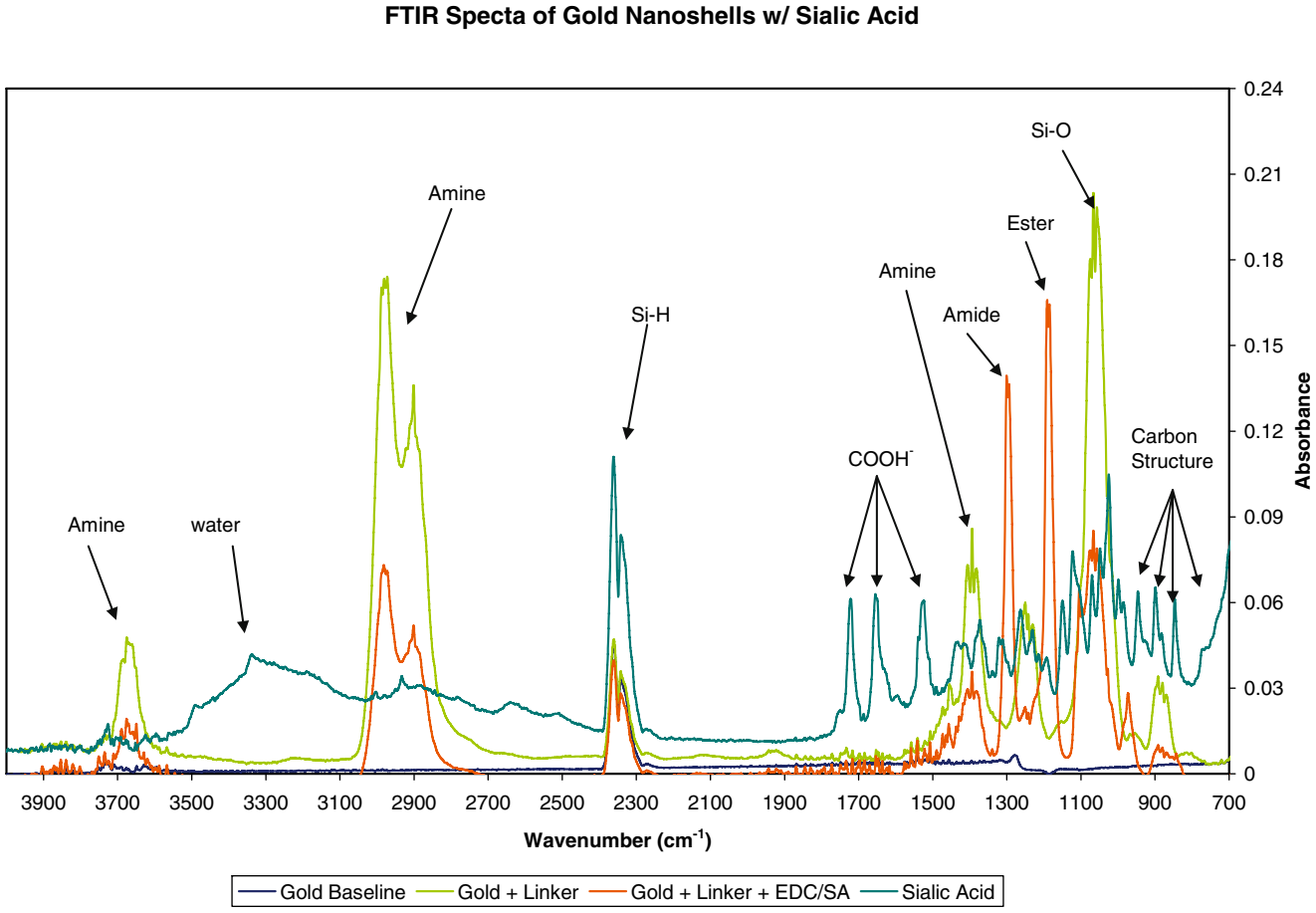

Fig. 2 Grazing angle FTIR spectra showing chemistry associated with the production of a multivalent sialic acid surface on gold. Notable peaks include the amide associated with bonding of a carboxylic acid with a primary amine through EDC chemistry, as well as the disappearance of the carboxylic acid and primary amine after the addition of EDC but the retention of carbon structure

and sialic acid in solution prior to attachment to the nanoshell surface, as these surfaces had fewer defects and less nonspecific Congo red binding.

Determination of binding affinity ($K_{A\beta}$) and surface saturation (N_{sat})

Figure 3 shows a representative binding isotherm for Aβ binding to the nanoshell substrates. The maximum binding of beta amyloid to the gold was estimated to be 0.7± 0.3 pmol/cm^2 of area of the slide coated with nanoshells, and the equilibrium dissociation constant of the Aβ with the surfaces was 14±8 nM. Two other proteins, lysozyme, which is known to form fibrils, and aprotinin, a small β-sheet protein, did not exhibit significant binding to the substrates. The Aβ binding affinity to sialic acid-modified surfaces is comparable to that of Aβ to sialic acid-modified dendrimers [18] and at least an order of magnitude greater than that measured for Aβ with the sialic acid containing glycolipids of cell membranes [7]. These results are significant in that they show that the Aβ is binding specifically to the sialic acid-modified nanoshell surfaces and that other proteins that form structures similar to Aβ do not bind appreciably under the same conditions.

Determination of SERS enhancement

Aβ by itself is not sufficiently SERS-active to enable direct measurement of Aβ on a surface. However, Aβ, in an extended β-sheet conformation, is known to bind Congo red, whose aromatic structure is SERS-active [60]. We therefore decided to examine the feasibility of utilizing a sandwich assay format, in which Aβ bound specifically to the sialic acid-modified surface, after which Congo red would bind specifically to Aβ, for the structure-specific detection of Aβ. Figure 4 demonstrates the Congo red signal obtained from functionalized nanoshells with 10 nM Aβ applied to the surface compared to the Congo red signal obtained from functionalized Platypus™ Gold-coated silicon wafers with the same concentration of Aβ. The Platypus wafers have a very smooth gold surface that does not have the necessary roughness for SERS enhancement. Using the smooth Platypus surfaces, no difference in signal from Aβ plus Congo red vs. the signal obtained from the gold surfaces with no Aβ or Congo red was observed. Thus, the necessity of using a SERS substrate such as the nanoshells is apparent. From the nanoshell spectra, it can be easily seen that Congo red has five identifiable peaks. Tentative band assignments for these peaks are based on current literature [59, 60]. The peaks at 1,155 and 1,595 cm^{-1} are related to the N–C stretch and phenyl-ring mode, respectively. The peaks from about 1,350 to 1,450 cm^{-1} are due to the contribution of the N=N stretching modes. Thus, the sandwich assay format in which Aβ is first added to the sialic acid-modified substrate, after which Congo red is bound to the Aβ, provides a meaningful signal for the detection of Aβ.

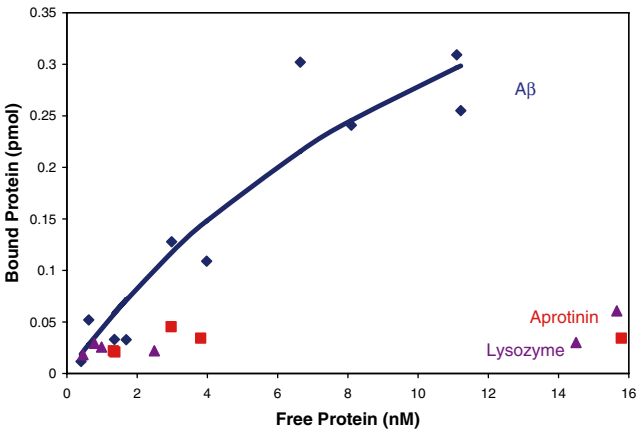

Fig. 3 Equilibrium binding isotherm of I-125-labeled Aβ bound to the sialic acid SAM. In this isotherm, the equilibrium dissociation constant of Aβ was determined to be 14±8 nM, and the maximum amount of Aβ bound to the surface was 0.7±0.3 pmol/cm^2 of area of the slide coated with nanoshells. It can be seen that aprotinin (*squares*) and lysozyme (*triangles*) do not bind to the substrates

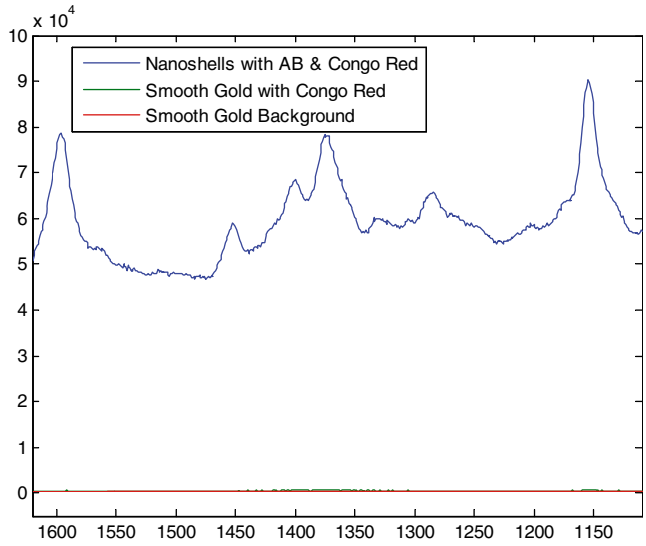

Fig. 4 Congo red spectra from functionalized slides with 10 nM Aβ applied to the surface. The *top spectrum* was taken from a nanoshell slide, whereas the *bottom spectra* are from a smooth gold surface with and without Congo red

Stability of SERS signal

One of the key features of using nanoshells for the SERS substrate is that the SERS enhancement is dependent on the surface plasmons of single nanoshells and not on clusters of particles. This feature is advantageous because it allows the signal to be consistent across the surface and to not depend

on local "hot spots," which make quantification difficult. Figure 5 (inset) shows the raw Congo red spectra taken for three consecutive scans from three random locations on a nanoshell slide with 10 nM Aβ bound to the surface. There are minor differences in these spectra; however, when corrected for differences in baseline intensity by dividing by the first intensity (which does not contain any Raman peaks), the spectra are very similar (Fig. 5 main). The intensities of the five major Congo red peaks were determined for each of the scans as shown in the table, with the largest percent deviation between the largest and smallest values for each peak found to be a maximum of 3.3%. This result indicates that the enhancement is consistent across the nanoshell surface, which allows for the potential for quantitative measures to relate SERS intensity with analyte concentration. It should be noted that the signal is more stable for nanoshell substrates with a thin layer of gold prior to nanoshell deposition. The gold layer greatly increases the Raman signal, most likely due to its reflective nature and possible coupling of the plasmon resonance of the nanoshells into the plasmon resonance of the gold surface, which allows for the use of the lower-magnification objective (10× instead of 20×) to obtain clear Raman spectra. The increased stability for a larger spot size indicates that part of the stability comes from the ability to take an average signal from a large number of nanoshells. As the manufacturing of the nanoshell substrates and the deposition of the chemistry and analytes on them continue to improve, the signals should remain or become more stable across the platform surface.

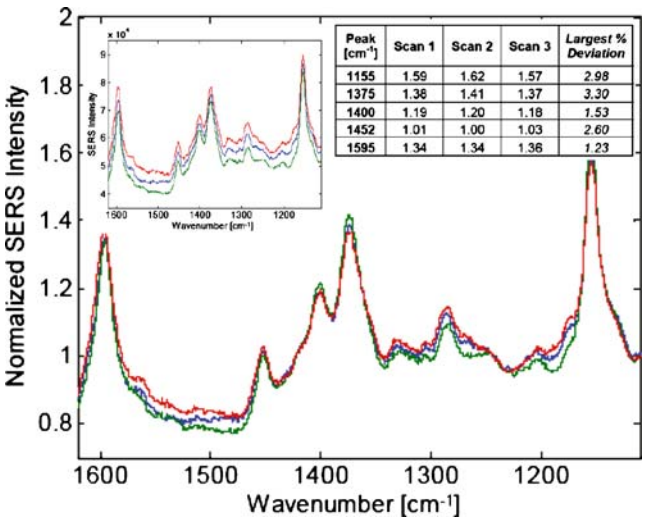

Peak [cm⁻¹]	Scan 1	Scan 2	Scan 3	Largest % Deviation
1155	1.59	1.62	1.57	2.98
1375	1.38	1.41	1.37	3.30
1400	1.19	1.20	1.18	1.53
1452	1.01	1.00	1.03	2.60
1595	1.34	1.34	1.36	1.23

Fig. 5 Congo red spectra showing the reproducibility of the SERS enhancement between random locations on the nanoshell slides. The *inset spectra* are the raw spectra that show slight differences in background intensity. When the difference in background intensity is corrected for, the spectra show at most a 3.3% deviation in peak height

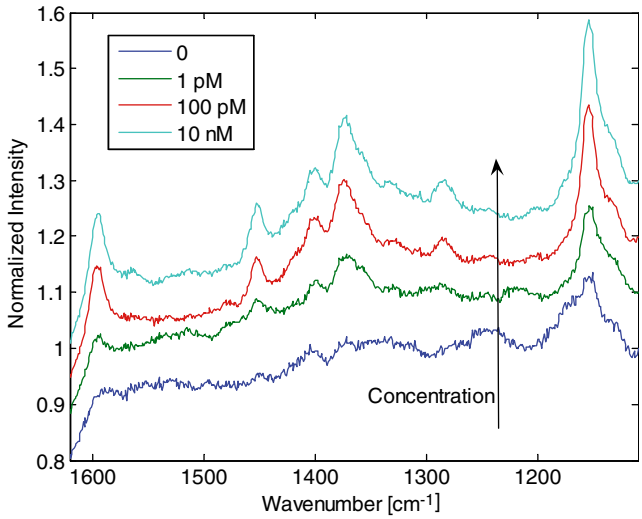

Fig. 6 Congo red spectra showing the spectra dependence on concentration of Aβ applied to the nanoshells. Concentrations as low as 1 pM Aβ plus Congo red show some spectral features. Greater peak intensity and refinement are observed as Aβ concentration increases. The *spectra* were slightly offset to more clearly show their differences

Aβ concentration using SERS

To analyze the ability of the SERS signal obtained from functionalized nanoshell slides to be used as a measure of Aβ, we looked at the signals obtained from several decreasing concentrations. We first applied Aβ to the slides, allowed it to bind, and rinsed off any excess. We then allowed a constant amount of Congo red to bind to the Aβ before any excess of that too was rinsed off. Figure 6,

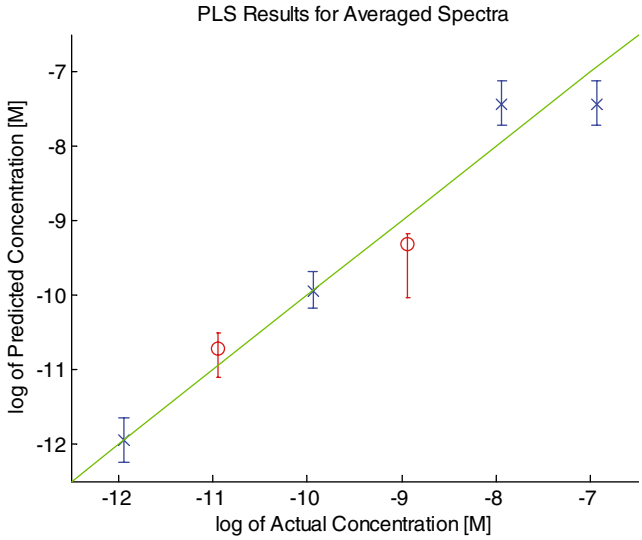

Fig. 7 Partial least squares results using two latent variables (*x*, calibration data; *o*, validation data) for Aβ in the picomolar to nanomolar range showing the signal dependence on the Aβ concentration. At around 10 nM, the signal levels off, indicating saturation of the nanoshell substrates. The *error bars* indicate the entire spread of the data at each concentration

which shows the Congo red signal corresponding to several concentrations of Aβ, demonstrates that we were able to detect peaks from Congo red bound to Aβ on the functionalized nanoshell surfaces at concentrations as low as 1 pM. For this figure, three spectra were averaged and normalized to the first point in the spectra, which does not include any Raman peaks, to account for slight differences in initial background intensity, as was done for the stability study. The spectra were then slightly offset so that their differences could be more clearly seen. In addition to reading levels to 1 pM, as the concentration of Aβ increased, the Congo red peaks became larger and more defined, showing a dependence of the Congo red signal on the Aβ concentration. This result was further examined by fitting the raw spectra to a partial least squares model with two latent variables (Fig. 7). The error bars indicate the entire spread of the data at each concentration; these spectra were taken with a small spot size on slides not precoated with a layer of gold so these results may be improved by using the gold-coated slides. At around 10 nM, the signal begins to saturate, indicating that the maximum amount of Aβ was bound to this point. This result complements the results obtained from the binding isotherm (Fig. 3), which indicates that the signal was coming from the Aβ and not from the nonspecific binding of Congo red to the surface. Although we are not at the point of definitive determination of Aβ concentration, we are able to detect the presence of Aβ oligomers in the picomolar to nanomolar range with indication of the possibility for more concentration-dependent detection with our current platforms.

Conclusions

In this paper, we have successfully functionalized slides consisting of a monolayer of nanoshells, optimized for our excitation laser wavelength, with chemistry specific for binding of Aβ. The sialic acid residues conjugated to nanoshells were shown to have a high affinity for Aβ with specificity for Aβ over other fibril-forming proteins. We also demonstrated the feasibility of using SERS to detect Aβ by monitoring the signal from Congo red bound to the Aβ on the slides and that this signal was consistent across various locations on the slides. In addition, we produced SERS spectra that indicate the feasibility of detecting Aβ oligomers into the picomolar range.

Acknowledgements The authors acknowledge the support of the National Institutes of Health (grant no. STTR-1R41AG025586-01 and grant no. R21-NS050346-01). The authors acknowledge the support of the Air Force (STTR FA9550-05-C-0019). Hope Beier acknowledges the support of a National Science Foundation Graduate Research Fellowship.

References

1. Ferri CP, Prince M, Brayne C, Brodaty H, Fratiglioni L, Ganguli M, Hall K, Hasegawa K, Hendrie H, Huang YQ, Jorm A, Mathers C, Menezes PR, Rimmer E, Scazufca M (2005) Global prevalence of dementia: a Delphi consensus study. Lancet 366(9503):2112–2117
2. Hebert LE, Scherr PA, Bienias JL, Bennett DA, Evans DA (2003) Alzheimer disease in the US population-prevalence estimates using the 2000 census. Arch Neurol 60(8):1119–1122
3. Hardy J, Selkoe DJ (2002) The amyloid hypothesis of Alzheimer's disease: progress and problems on the road to therapeutics. Science 297:353–356
4. Minino AM, Heron MP, Smith BL (2006) Deaths: preliminary data for 2004. Natl Vital Stat Rep 54(19):1–50
5. Selkoe DJ (2001) Alzheimer's disease: genes, proteins, and therapy. Physiol Rev 81(2):741–766
6. Ernst RL, Hay JW (1994) The U.S. economic and social costs of Alzheimer's disease revisited. Am J Public Health 84(8):1261–1264
7. Ariga T, Kobayashi K, Hasegawa A, Kiso M, Ishida H, Miyatake T (2001) Characterization of high-affinity binding between gangliosides and amyloid beta-protein. Arch Biochem Biophys 388(2):225–230
8. Bard F, Cannon C, Barbour R, Burke RL, Games D, Grajeda H, Guido T, Hu K, Huang JP, Johnson-Wood K, Khan K, Kholodenko D, Lee M, Lieberburg I, Motter R, Nguyen M, Soriano F, Vasquez N, Weiss K, Welch B, Seubert P, Schenk D, Yednock T (2000) Peripherally administered antibodies against amyloid beta-peptide enter the central nervous system and reduce pathology in a mouse model of Alzheimer disease. Nat Med 6(8):916–919
9. Bergamaschini L, Rossi E, Storini C, Pizzimenti S, Distaso M, Perego C, De Luigi A, Vergani C, De Simoni MG (2004) Peripheral treatment with enoxaparin, a low molecular weight heparin, reduces plaques and beta-amyloid accumulation in a mouse model of Alzheimer's disease. J Neurosci 24(17):4181–4186
10. Blanchard BJ, Chen A, Rozeboom LM, Stafford KA, Weigele P, Ingram VM (2004) Efficient reversal of Alzheimer's disease fibril formation and elimination of neurotoxicity by a small molecule. Proc Natl Acad Sci USA 101(40):14326–14332
11. DeMattos RB, Bales KR, Cummins DJ, Dodart JC, Paul SM, Holtzman DM (2001) Peripheral anti-A beta antibody alters CNS and plasma A beta clearance and decreases brain A beta burden in a mouse model of Alzheimer's disease. Proc Natl Acad Sci USA 98(15):8850–8855
12. Etcheberrigaray R, Tan M, Dewachter I, Kuiperi C, Van der Auwera I, Wera S, Qiao LX, Bank B, Nelson TJ, Kozikowski AP, Van Leuven F, Alkon DL (2004) Therapeutic effects of PKC activators in Alzheimer's disease transgenic mice. Proc Natl Acad Sci USA 101(30):11141–11146
13. Gelinas DS, DaSilva K, Fenili D, George-Hyslop PS, McLaurin J (2004) Immunotherapy for Alzheimer's disease. Proc Natl Acad Sci USA 101:14657–14662
14. Ghanta J, Shen CL, Kiessling LL, Murphy RM (1996) A strategy for designing inhibitors of beta-amyloid toxicity. J Biol Chem 271(47):29525–29528
15. Hock C, Konietzko U, Streffer JR, Tracy J, Signorell A, Muller-Tillmanns B, Lemke U, Henke K, Moritz E, Garcia E, Wollmer MA, Umbricht D, de Quervain DJF, Hofmann M, Maddalena A, Papassotiropoulos A, Nitsch RM (2003) Antibodies against beta-amyloid slow cognitive decline in Alzheimer's disease. Neuron 38(4):547–554
16. Mandavilli A (2006) The amyloid code. Nat Med 12(7):747–751
17. Mount C, Downton C (2006) Alzheimer disease: progress or profit? Nat Med 12(7):780–784

18. Patel D, Henry J, Good T (2006) Attenuation of beta-amyloid induced toxicity by sialic acid-conjugated dendrimeric polymers. Biochim Biophys Acta 1760(12):1802–1809
19. Brookmeyer R, Gray S, Kawas C (1998) Projections of Alzheimer's disease in the United States and the public health impact of delaying disease onset. Am J Public Health 88(9):1337–1342
20. Davis PC, Gray L, Albert M, Wilkinson W, Hughes J, Heyman A, Gado M, Kumar AJ, Destian S, Lee C, Duvall E, Kido D, Nelson MJ, Bello J, Weathers S, Jolesz F, Kikinis R, Brooks M (1992) The consortium to establish a registry for Alzheimers-disease (Cerad) .3. Reliability of a standardized Mri evaluation of Alzheimers-disease. Neurology 42(9):1676–1680
21. Duara R, Grady C, Haxby J, Sundaram M, Cutler NR, Heston L, Moore A, Schlageter N, Larson S, Rapoport SI (1986) Positron emission tomography in Alzheimers-disease. Neurology 36 (7):879–887
22. Haxby JV, Grady CL, Duara R, Schlageter N, Berg G, Rapoport SI (1986) Neocortical metabolic abnormalities precede non-memory cognitive defects in early Alzheimers-type dementia. Arch Neurol 43(9):882–885
23. Blennow K (2004) CSF biomarkers for mild cognitive impairment. J Intern Med 256:224–234
24. Mattson MP, Mark RJ, Furukawa K, Bruce AJ (1997) Disruption of brain cell ion homeostasis in Alzheimer's disease by oxy radicals, and signaling pathways that protect therefrom. Chem Res Toxicol 10(5):507–517
25. Rapport M, Dawson HN, Binder LI, Vitek MP, Ferreira A (2002) Tau is essential to β-amyloid-induced neurotoxicity. Proc Natl Acad Sci USA 99:6364–6369
26. Small GW (2002) Brain-imaging surrogate markers for detection and prevention of age-related memory loss. J Mol Neurosci 19(1–2):17–21
27. Varadarajan S, Yatin S, Aksenova M, Butterfield DA (2000) Review: Alzheimer's amyloid β-peptide-associated free radical oxidative stress and neurotoxicity. J Struct Biol 130:184–208
28. Walsh DM, Klyubin I, Fadeeva JV, Rowan MJ, Selkoe DJ (2002) Amyloid-beta oligomers: their production, toxicity and therapeutic inhibition. Biochem Soc Trans 30:552–557
29. Wang SSS, Rymer DL, Good TA (2001) Reduction in cholesterol and sialic acid content protects cells from the toxic effects of beta-amyloid peptides. J Biol Chem 276(45):42027–42034
30. Zetterberg H, Wahnlund L-O, Blennow K (2003) Cerebrospinal fluid markers for prediction of Alzheimer's disease. Neurosci Lett 352:67–69
31. Cleary JP, Walsh DM, Hofmeister JJ, Shankar GM, Kuskowski MA, Selkoe DJ, Ashe KH (2005) Natural oligomers of the amyloid-protein specifically disrupt cognitive function. Nat Neurosci 8(1):79–84
32. Gong Y, Chang L, Viola KL, Lacor PN, Lambert MP, Finch CE, Krafft GA, Klein WL (2003) Alzheimer's disease-affected brain: presence of oligomeric Aβ ligands (ADDLs) suggests a molecular basis for reversible memory loss. Proc Natl Acad Sci USA 100 (18):10417–10422
33. Hardy J, Selkoe DJ (2002) Medicine—the amyloid hypothesis of Alzheimer's disease: progress and problems on the road to therapeutics. Science 297(5580):353–356
34. Lee S, Fernandez EJ, Good TA (2007) Role of aggregation conditions in structure, stability, and toxicity of intermediates in the Aβ fibril formation pathway. Protein Sci 16(4):723–732
35. Lorenzo A, Yankner BA (1994) Beta-amyloid neurotoxicity requires fibril formation and is inhibited by Congo red. Proc Natl Acad Sci USA 91(25):12243–12247
36. Selkoe DJ, Schenk D (2003) Alzheimer's disease: molecular understanding predicts amyloid-based therapeutics. Annu Rev Pharmacol Toxicol 43:545–584
37. Haes AJ, Chang L, Klein WL, Van Duyne RP (2005) Detection of a biomarker for Alzheimer's disease from synthetic and clinical samples using a nanoscale optical biosensor. J Am Chem Soc 127 (7):2264–2271
38. Haes AJ, Hall WP, Chang L, Klein WL, Van Duyne RP (2004) A localized surface plasmon resonance biosensor: first steps toward an assay for Alzheimer's disease. Nano Lett 4(6):1029–1034
39. Georganopoulou DG, Chang L, Nam JM, Thaxton CS, Mufson EJ, Klein WL, Mirkin CA (2005) Nanoparticle-based detection in cerebral spinal fluid of a soluble pathogenic biomarker for Alzheimer's disease. Proc Natl Acad Sci USA 102(7):2273–2276
40. Kneipp K, Wang Y, Kneipp H, Perelman LT, Itzkan I, Dasari R, Feld MS (1997) Single molecule detection using surface-enhanced Raman scattering (SERS). Phys Rev Lett 78(9):1667–1670
41. Kneipp K, Wang Y, Kneipp H, Itzkan I, Dasari RR, Feld MS (1996) Population pumping of excited vibrational states by spontaneous surface-enhanced Raman scattering. Phys Rev Lett 76(14):2444–2447
42. Nie SM, Emery SR (1997) Probing single molecules and single nanoparticles by surface-enhanced Raman scattering. Science 275 (5303):1102–1106
43. Fleischmann M, Hendra PJ, McQuillan AJ (1973) Raman-spectra from electrode surfaces. J Chem Soc Chem Commun (3):80–81
44. Jeanmaire DL, Vanduyne RP (1977) Surface raman spectroelectrochemistry. 1. Heterocyclic, aromatic, and aliphatic-amines adsorbed on anodized silver electrode. J Electroanal Chem 84 (1):1–20
45. Baker GA, Moore DS (2005) Progress in plasmonic engineering of surface-enhanced Raman-scattering substrates toward ultra-trace analysis. Anal Bioanal Chem 382(8):1751–1770
46. Kneipp K, Kneipp H, Itzkan I, Dasari RR, Feld MS (2002) Surface-enhanced Raman scattering and biophysics. J Phys Condens Matter 14(18):R597–R624
47. Oldenburg SJ, Jackson JB, Westcott SL, Halas NJ (1999) Infrared extinction properties of gold nanoshells. Appl Phys Lett 75 (19):2897–2899
48. Jackson JB, Halas NJ (2003) Controlling the surface enhanced Raman effect on nanoshells in a film geometry. Abstr Pap Am Chem Soc 225:U447
49. Jackson JB, Halas NJ (2004) Surface-enhanced Raman scattering on tunable plasmonic nanoparticle substrates. Proc Natl Acad Sci USA 101(52):17930–17935
50. Oldenburg SJ, Westcott SL, Averitt RD, Halas NJ (1999) Surface enhanced Raman scattering in the near infrared using metal nanoshell substrates. J Chem Phys 111(10):4729–4735
51. Zhu ZH, Zhu T, Liu ZF (2004) Raman scattering enhancement contributed from individual gold nanoparticles and interparticle coupling. Nanotechnology 15(3):357–364
52. Li KR, Stockman MI, Bergman DJ (2003) Self-similar chain of metal nanospheres as an efficient nanolens. Phys Rev Lett 91(22)
53. ChooSmith LP, GarzonRodriguez W, Glabe CG, Surewicz WK (1997) Acceleration of amyloid fibril formation by specific binding of A beta-(1–40) peptide to ganglioside-containing membrane vesicles. J Biol Chem 272(37):22987–22990
54. Kakio A, Nishimoto S, Yanagisawa K, Kozutsumi Y, Matsuzaki K (2001) Cholesterol-dependent formation of GM1 ganglioside-bound amyloid beta-protein, an endogenous seed for Alzheimer amyloid. J Biol Chem 276(27):24985–24990
55. Kakio A, Yano Y, Takai D, Kuroda Y, Matsumoto O, Kozutsumi Y, Matsuzaki K (2004) Interaction between amyloid beta-protein aggregates and membranes. J Pept Sci 10(10):612–621
56. Matsuzaki K, Horikiri C (1999) Interactions of amyloid beta-peptide (1–40) with ganglioside-containing membranes. Biochemistry 38(13):4137–4142

57. Wakabayashi M, Okada T, Kozutsumi Y, Matsuzaki K (2005) GM1 ganglioside-mediated accumulation of amyloid beta-protein on cell membranes. Biochem Biophys Res Commun 328(4):1019–1023
58. Williamson MP, Suzuki Y, Bourne NT, Asakura T (2006) Binding of amyloid beta-peptide to ganglioside micelles is dependent on histidine-13. Biochem J 397:483–490
59. Iconomidou VA, Chryssikos GD, Gionis V, Hoenger A, Hamodrakas SJ (2003) FT-Raman spectroscopy as diagnostic tool of Congo red binding to amyloids. Biopolymers 72(3):185–192
60. Miura T, Yamamiya C, Sasaki M, Suzuki K, Takeuchi H (2002) Binding mode of Congo red to Alzheimer's amyloid beta-peptide studied by UV Raman spectroscopy. J Raman Spectrosc 33(7):530–535
61. Khurana R, Uversky VN, Nielsen L, Fink AL (2001) Is Congo red an amyloid-specific dye? J Biol Chem 276(25):22715–22721